International Conference on Space Optics—ICSO 2022

Dubrovnik, Croatia

3–7 October 2022

Edited by Kyriaki Minoglou, Nikos Karafolas, and Bruno Cugny,

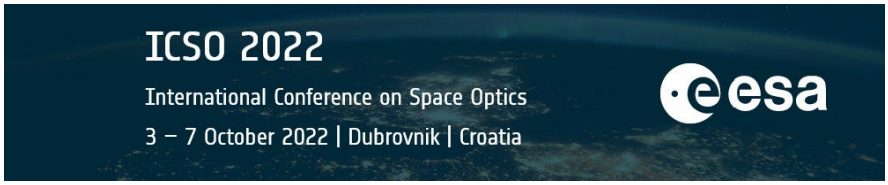

Design and Analysis of Filter assemblies for the LSTM Instrument

International Conference on Space Optics — ICSO 2022, edited by Kyriaki Minoglou, Nikos Karafolas, Bruno Cugny, Proc. of SPIE Vol. 12777, 127776C · © 2023 ESA and CNES · 0277-786X · doi: 10.1117/12.2691124

Design and Analysis of Filter assemblies for the LSTM Instrument

Matthias Mohaupt*[a], Christian Scheffler[a], Falk Kemper[a], Gerd Harnisch[a], Max Henning[b], Andreas Rahm[b], Olivier Sengenès[c], Bruno Badoil[c], Pierre-Olivier Antoine[c], Emilie Steck[c]

[a]Fraunhofer Institute for Applied Optics and Precision Engineering, Albert-Einstein-Strasse 7, D-07745 Jena, Germany;
[b]Materion Balzers Optics – Optics Balzers Jena GmbH, Otto-Eppenstein-Str. 2, D-07745 Jena, Germany;
[c]Airbus Defence and Space, 31 rue des Cosmonautes, 31402 Toulouse Cedex 4, France

*matthias.mohaupt@iof.fraunhofer.de; www.iof.fraunhofer.de

ABSTRACT

LSTM, funded by the EU and ESA, is part of Copernicus, the European Union's Earth observation program for global monitoring. It is one of the six new missions, expanding the capabilities of the current Copernicus space component.

The Copernicus Land Surface Temperature Monitoring, LSTM, mission carries a high spatial-temporal resolution thermal infrared sensor to provide observations of land-surface temperature. The mission responds to priority requirements of the agricultural user community for improving sustainable agricultural productivity at field-scale in a world of increasing water scarcity and variability. Land-surface temperature measurements and derived evapotranspiration are key variables to understand and respond to climate variability, manage water resources for agricultural production, predict droughts, and to address land degradation, natural hazards such as fires and volcanoes, coastal and inland water management as well as urban heat island issues [1].

The LSTM satellite is designed and build by Airbus DS in Madrid, while the development and production of the advanced technology instrument is carried out by Airbus DS in Toulouse. The detector plane filter (DPF) assemblies for the SWIR and VIS detector and the filter assembly for intermediate plane filters VNIR (IPF-VNIR) are developed, manufactured, integrated, and tested by Fraunhofer IOF. Optic Balzers Jena (OBJ) is the responsible subcontractor for the VNIR/SWIR filter assemblies and will provide the optical filter coatings.

The design of filter assemblies for the detector plane filters of SWIR detector (DPF-SWIR) is developed. The filter assemblies consist of a lower frame and upper frame. Four single filter substrates coated with the bandpass filter layers are integrated into the lower frame. The upper and lower mask apertures are integrated into the upper and lower frame.

The design of DPF-SWIR filter assemblies was analyzed by finite element (FE) analysis. The mechanical loads of sine and random vibration and shock are calculated. The modal analysis shows the meet of requirements of first eigenfrequency. The mechanical loads of interface imperfections are analyzed. The thermal loads are also analyzed, in combination with interface mechanical loads. In sum 21 load cases are investigated.

Keywords: detector plane filter assembly, mechanical design, thermal analysis, structural analysis, LSTM instrument

1. LSTM MISSION DESCRIPTION

LSTM, funded by the EU and ESA, is part of Copernicus, the European Union's Earth observation program for global monitoring. It is one of the six new missions, expanding the capabilities of the current Copernicus space component.

The Copernicus Land Surface Temperature Monitoring, LSTM, mission carries a high spatial-temporal resolution thermal infrared sensor to provide observations of land-surface temperature. The mission responds to priority requirements of the agricultural user community for improving sustainable agricultural productivity at field-scale in a world of increasing water scarcity and variability. Land-surface temperature measurements and derived evapotranspiration are key variables to understand and respond to climate variability, manage water resources for agricultural production, predict droughts, and to address land degradation, natural hazards such as fires and volcanoes, coastal and inland water management as well as urban heat island issues [1].

Figure 1. LSTM image, source ESA [1]

The LSTM satellite, see figure 1, is designed and build by Airbus DS in Madrid, while the development and production of the advanced technology instrument is carried out by Airbus DS in Toulouse. The detector plane filter (DPF) assemblies for the SWIR and VIS detector and the filter assembly for intermediate plane filters VNIR (IPF-VNIR) is developed, manufactured, integrated, and tested by Fraunhofer IOF. Optic Balzers Jena (OBJ) is the responsible subcontractor for the VNIR/SWIR filter assemblies and will provide the coatings.

2. LSTM INSTRUMENT DESCRIPTION

The LSTM instrument mainly includes a scanning mirror, a telescope and dichroic beam-splitter-1, which separates beams towards, see figure 2:

- the TIR path with TIR imaging camera including optics, TIR bandpass and background filters (IPF-TIR and DPF-TIR) and detectors
- the VNIR-SWIR path, itself split in 2 new paths thanks to dichroic beam-splitter-2:
    - NIR-SWIR focal plane with NIR-SWIR filters and detectors on dichroic-2 transmitted path
    - VIS focal plane with VIS filters and detectors on dichroic beam-splitter-2 reflected path.

The bandpass is shaped by a first stage of filtering, carried by IPF. The background is rejected, and the crosstalk is minimized thanks to a second stage of filtering, carried by the DPF.

On VNIR-SWIR paths, the first common stage is with IPF-VNIR/SWIR filters located close to dichroic beam-splitter-1, while the filtering is completed with DPF-SWIR and DPF-VIS respectively, located in the front of the detectors.

On TIR path, IPF-TIR is located close to dichroic beam-splitter-1 and DPF-TIR is located in the front of the detector.

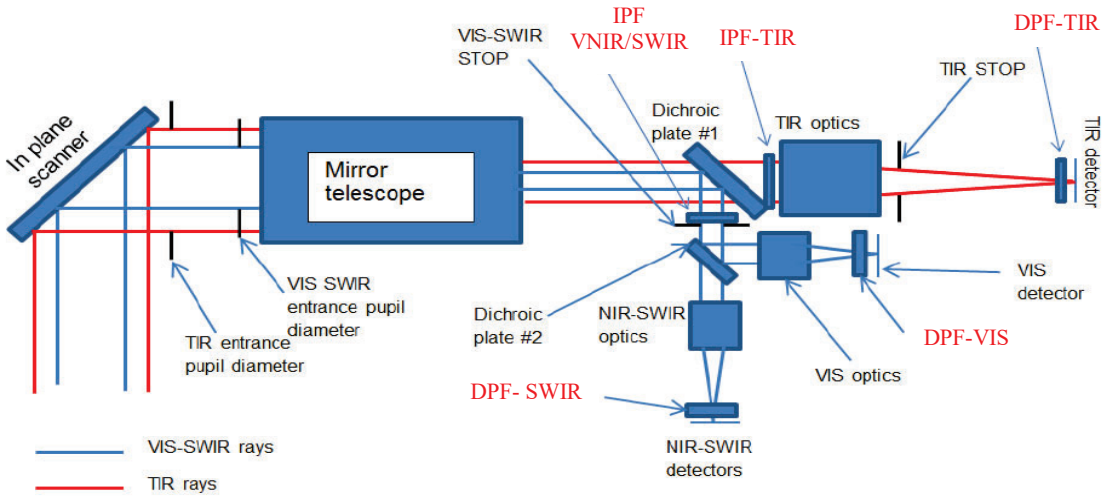

Figure 2: optical system design of LSTM instrument: Preliminary optical layout of the instrument [2]

Each mounted filter unit includes strip filters dedicated to several spectral bands from Table 1 below. IPF units are large strip filters operating under low incidence angles and with high F-number beams, while DPF units are smaller strip filters operating under a wide range of incidence angles and with low F-number beams.

Table 1: LSTM instrument spectral bands

Band	Central wavelength λ_c (nm)	Width FWHM (nm)
VNIR-0	490	65
VNIR-1	665	30
VNIR-2	865	20
VNIR-3 a/b	945	20
SWIR-1	1380	30
SWIR-2	1610	90
TIR-1	8600	180
TIR-2	8900	180
TIR-3	9200	180
TIR-4	10900	400
TIR-5	12000	470

Each filter assembly includes one mask on each side of the strips in order to limit straylight and parasitic images propagation.

3. DESIGN CONCEPT OF LSTM FILTER ASSEMBLIES

3.1 Design Heritage Sentinel 2 MSI – SWIR and VNIR Filter Assemblies

In the frame of the Sentinel-2 – GMES-mission (in cooperation with instrument prime Airbus Defence and Space Toulouse), Fraunhofer IOF has been a supplier of Jena Optronik GmbH and was responsible for the manufacturing and the integration of the VNIR- and SWIR filter arrays. Optics Balzers Jena GmbH (OBJ) was responsible for spectral filter coatings. The manufacturing and the integration concept for SWIR- and VNIR filter assemblies, see figures 3 and 4, was developed during a Phase B Study [5] and was proven at the Phase C/D [6]. The Sentinel-2A satellite was launched in June 2015 and works successful. The Sentinel-2B satellite was launched in March 2017. Fraunhofer IOF has been working on the realization of the Sentinel-2C and -2D filter assemblies until 2018.

3.2 Mounting concept of filter arrays for Sentinel 2

The single filter elements are arranged into mechanical subassemblies made of titanium alloys and were aligned into the optical instrument in front of the detectors. During the integration of the single filter elements to filter arrays, the optical elements will be arranged into the mechanical holders with positioning accuracies of less than 10 µm. The optical apertures were realized by high precision manufacturing of the mechanical parts. Manufacturing accuracies of the functional opto-mechanical structures of less than ± 15 µm were achieved [7].

Figure 3: VNIR (left) and SWIR (right) Filter Array for Sentinel 2 Multispectral Imager (MSI). [7]

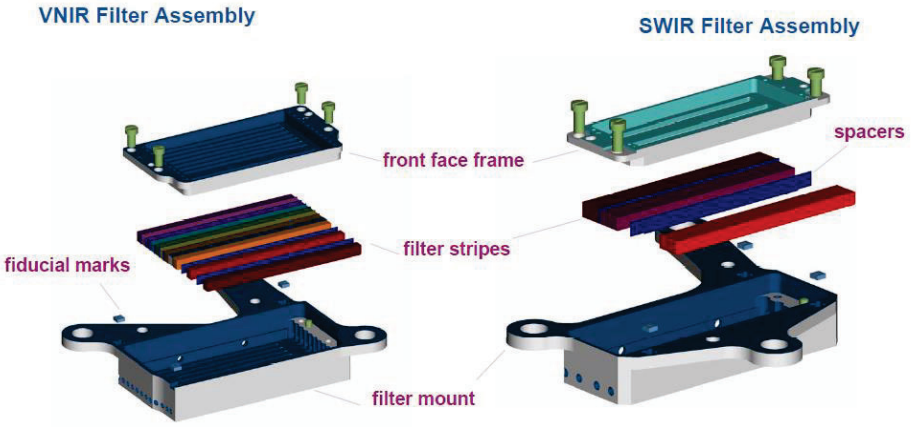

Figure 4: VNIR (left) and SWIR (right) filter assemblies – exploded assembly drawings

3.3 Design Baseline for LSTM DPF-SWIR Filter assemblies

The general design baseline for LSTM filter assemblies is to use as much as possible heritage in design, materials, and processes from Sentinel 2 MSI SWIR filter assemblies. The following design baseline was used during design development for LSTM DPF-SWIR filter assemblies:

- Upper and lower frame (Titanium-Alloy) for mechanical mounting single filter stripes (substrates)
- Clear apertures integrated into upper and lower frame – optical apertures
- Single Filter stripes positioned on hard mechanical stops at lower frames
- Fixation of single filter stripes by an elastic adhesive as filler
- Sheets of metal for channel separation (stainless-steel, black coated)
- Fiducial marks on lower frame for aperture position measurements
- Positioning of upper frame to lower frame by pins and holes
- Black coating of outside surfaces of mechanical parts by Acktar.

4. DESIGN OF DPF-SWIR FILTER ASSEMBLIES

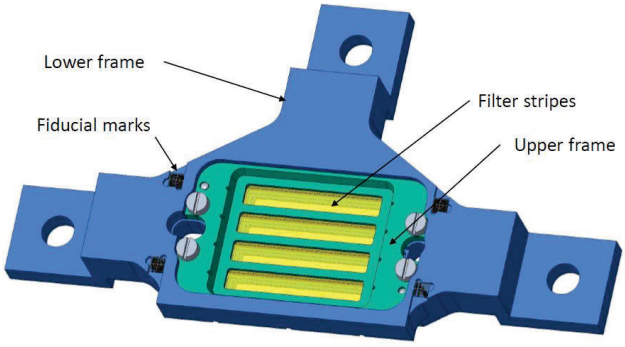

Figure 5: design of DPF-SWIR filter assembly (isometric view)

The components of DPF-SWIR filter assemblies are the lower frame (blue part) and the upper frame (green part), see figure 5. The upper frame is integrated into lower frame. Mechanical pins are used for positioning, the fixation is done by screws. Four filter substrates, VNIR-3a, VNIR-3b, SWIR 1 and SWIR 2 will be integrated into lower frame.

The single filter substrates will be separated by mechanical spacer foils of stainless-steel with black coatings on each side. The single filter stripes will be fixed by an elastic filler adhesive by filling the gaps in between the filter stripes and the pockets of lower frame (red dots), see figure 6. After insertion of upper frame, the gaps in between the upper frame and the top of the filter stripes will be filled with elastic filler adhesive, too.

Four fiducial marks with lithographic structured cross structures will be used for measurement- and alignment tasks. Thus, the position of the filter assembly and the upper and lower masks position with respect to the mechanical interface will be verified and can be used during integration and alignment of DPF-SWIR filter assembly into the focal plane array.

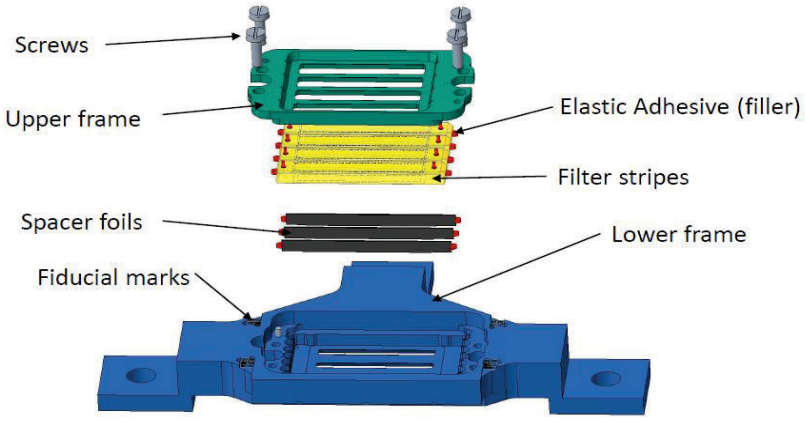

Figure 6: DPF-SWIR filter assembly – exploded view

5. DYNAMIC AND THERMO- MECHANICAL ANALYSIS OF DPF-SWIR AND DPF-VIS FILTER ASSEMBLIES

Optical instruments which are used as flight hardware in satellites and spacecrafts encounter mechanical shocks and vibration from a variety of sources. Launch vehicles typically cause most of the critical dynamic load steps to the payload. Furthermore, thermal loads of space components in orbit must be considered. Although, satellites have a sophisticated thermal management, some IR applications require cryogenic operation of optical components which sometimes poses challenging thermal loads. The following quasistatic, dynamic, and thermal loads have been investigated for the DPF-SWIR and DPF-VIS filter assembly:

- Quasistatic acceleration load: 1g can be considered as gravitation release in orbit. In this load case deformations of the filter strips are of interest because the assembly of the component is done under 1g earth gravity. Furthermore, a quasistatic load of 70g was investigated which covers all bulk accelerations of the rocket, e.g. average of acceleration during launch, as well as contributions of any random vibration significantly below the natural frequency of the payload or the specific component in the payload. However, the 70g load step do not yield critical stresses in our analysis on the filter assembly, hence it is not discussed in this paper.
- Sine displacement load: Sine loads have not been investigated for the DPF-SWIR assembly, as the lowest eigenfrequency of the system is far beyond the usual 5-100Hz frequency range for sine loads. In some cases, sine load tests are required with specified displacement amplitudes at interface points in the low frequency range, typically between 5-25Hz and with acceleration amplitudes in a higher frequency range between 25-100Hz. However, if the first eigenfrequencies of the system (DPF-SWIR filter assembly appr. 630Hz) are significantly higher than these frequency ranges, the system behaves quasi-static and a quasi-static investigation with an acceleration body load is adequate.
- Random vibration load: During the early lift-off phase of a carrier rocket, e.g., Ariane 5, Soyuz, Falcon heavy, solid rocket boosters (SRB) are often used to increase thrust which typically lasts less than 150 seconds and burn-off of the SRB is far before MECO (Main Engine Cut Off) point. Due to pressure oscillations during burning of the rocket motor the launch vehicle structure and therefore also the payload is excited by a superposition of sinusoidal acceleration loads with multiple oscillation frequencies (usually in the range 150-1800Hz) or with transient acceleration loads. This loading can be best described as a so-called random vibration load which is characterized by a specific acceleration level usually expressed with a power spectral density diagram. Additionally, aerodynamic stresses at the fairing due to transonic shock oscillations at transonic speed and shock induced separation of pressure waves at supersonic speed are another source of excitations. Along with the shock load case, random vibration loading is one of the critical load cases in terms of stresses or fastener loading.
- Shock load: During launch of the carrier rocket the filter assembly must withstand a series of flight shock pulses. Particularly, shock loads have its origin in rocket motor ignition and cut off, staging and deployment events. Strong separation events occur when pyrotechnic fasteners are used to separate stages of multistage rockets but also the separation by pneumatic systems imposes significant shock loads due to the inertia of the rejected stages. Furthermore, jettisoning of payload fairing and the separation of the payload itself are other important sources of shock vibrations for space components. Launch vehicle structures tend to be less susceptible to shock loads due to large inertias, however sensitive optical components are generally be critical parts.
- 190K and 333K thermal load: The thermal environment for components might be extreme. Low temperatures are usually occurring as operational temperature for space components in orbit, but besides that they are also often required for components in IR applications to reduce thermal noise (cryogenic operational state). In contrast, high temperature levels can occur in different ground operation steps of the assembly (bake out, outgassing or simply transport) or within the launch because of heating on the fairing which eventually radiates to the payload. Decoupling of thermally induced deformations due to CTE (coefficient of thermal expansion) mismatch between the filter assembly and the base plate is realized and checked by the loading of interface points.

A summary of all investigated load steps of the DPF-SWIR assembly are given in Table 2. Three slightly differing models have been used which consider geometrical nonlinearities (contact) in the structure and the necessity to consider a base plate with a specified CTE in the thermal analyses.

Table 2. Load steps

LS	Load applied	Boundary conditions	Remarks
1-6	Acceleration 1 g and 70g in x, y, z	Interface areas fixed in 6 DOF via remote points	Equivalent to 70g sine load
7-10	PSD Spectrum in x, y, z	Interface areas are excitation points	
11-13	Response Spectrum in x, y, z	Interface areas are excitation points	
14-15	Temperature on all parts: 333K+5K and 190K-5K	Interface areas are fixed on a base plate with a specific CTE	Maximum bake-out temperature and minimum non-operational temperature
16-21	none	Offset of 20 µm in z on IF area #2, #3 Tilt of 0.048° about x, y on IF area #2, #3, all other DOF fixed	Simulation of interface imperfections

As mentioned, three different models were setup for all the numerical investigations (Figure 8). The model which is used in the dynamic analyses (Random vibration and Response spectrum analysis) is a fully linear mechanical model as both analyses based on modal data (eigenvectors and eigenfrequencies) of a preceding Modal analysis. It considers a fixed connection (merged nodes) between the filter stripes and the lower frame parts. In contrast, the model which is used for the thermal load steps and for the calculation of the interface defects is nonlinear as it assumes a frictionless contact between the lower frame part and the filter stripes and the spacers (Figure 7). Absence of friction was considered because this is a conservative assumption if no detailed friction coefficient data is available and because there are no rigid body modes of the filter strips and spacers possible (they are still connected to the housing via the adhesive). Hence, the contact between the filter stripes, spacers and the lower frame part solely serves to allow a relatively free touching of the filter stripes/spacers to the lower frame. Some minor simplifications were applied to the FEM model.

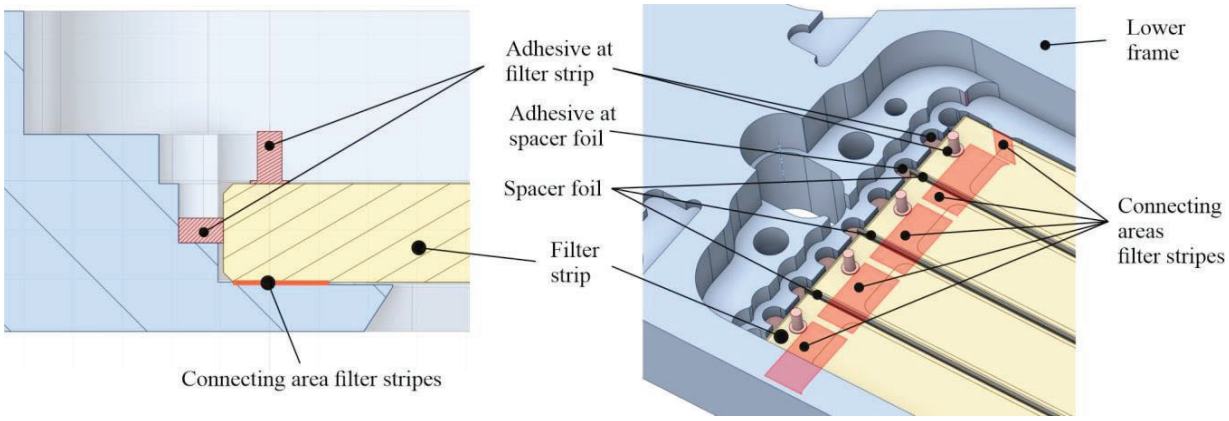

Figure 7: Depiction of the connecting area between filter stripes and housing. This area is modelled as a frictionless contact for the interface imperfection and thermal load case and have merged nodes for the linear dynamic load cases. Left: Cross section of a filter strip with adhesive and contact zone. Right: DPF-SWIR with suppressed upper housing part to reveal the view to the filter strips.

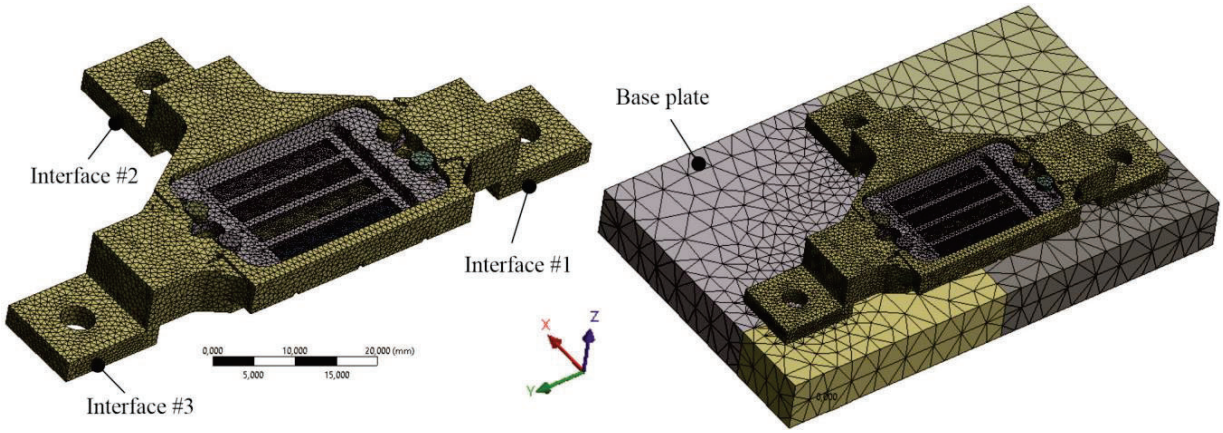

Figure 8: Left: FEM model of the LSTM filter assembly for the interface imperfection and dynamic load steps. Right: FEM model for the thermal load steps including the base plate with partitioning for application of displacement boundary conditions (y=0 in xz-plane, x=0 in yz-plane, z=0 in xy-plane at interface level).

The material properties in Table 3 were assumed for the simulation. Due to a lack of detailed material data of the adhesive of the filter stripes and spacers, the elastic modulus was calculated by a conversion from the known shore hardness. It must be mentioned that the elastic modulus of elastomer adhesives generally features elastic nonlinearity and a strong dependency on the temperature. Both nonlinearities were not considered due to lack of material data and the restriction to a linear analysis for the random vibration and response spectrum analyses. Furthermore, the tensile strength of the filter material strongly depends on the surface roughness, which is typical for glass materials. Hence a conservative value was applied. The total mass of the filter assembly is 31.4g.

Table 3: Assumed material properties.

Component	Housing	Filter	Spacer	Bolts	Adhesive
Material	Titanium alloy	Fused Silica	Stainless steel	Stainless steel	Elastic Adhesive
Young's modulus [GPa]	114	70	200	200	0.00353
Poisson number	0.34	0.17	0.3	0.3	0.45
Density [kg/m³]	4430	2200	7940	7940	1090
CTE [ppm/K]	8.5	0.3	16	16	200
Yield Strength [MPa]	830	-	210	210	-
Tensile Strength [MPa]	900	50	500	500	1.5

5.1 Modal analysis

Modal parameters are the base for all the conducted dynamic analyses, as the random vibration and response spectrum analysis based on a superposition of modal separated oscillations with their specific sensitivity, i.e. their contribution to the total dynamic system. This contribution of each mode is typically expressed by the participation factors or equivalently by the modal mass of each eigenmode. Hence, a modal analysis with fixed interfaces was performed prior to the dynamic analyses to consider all modes up to 32kHz (70 modes). The results of this analysis are given in Table 4. Due to the design of the filter assembly, a significant part of the mass in the vicinity of the interfaces can be regarded as

fixed “dead mass”, what means this mass is not dynamically active and do not contribute to modal masses in eigenmodes within the selected frequency range. This should be kept in mind when discussing the relatively low sum of the modal masses in the FEM model. However, the first 70 modes comprise all relevant mode shapes for the parts of interest.

Table 4: Modal results. Listed are only eigenmodes with a modal mass contribution >3% to the total mass.

Mode #	Frequency	Effective mass ratio [%]		
	[Hz]	x-direction	y-direction	z-direction
1	626	0.11	0.00	0.00
…				
9	**2279**	2.12	0.00	**60.99**
…				
14	**3430**	0.00	**75.38**	0.00
15	4473	8.53	0.00	0.00
16	**4570**	**28.36**	0.00	0.65
17	**4646**	**41.84**	0.00	0.97
…				
38	14700	0.00	0.00	3.10
…				
68	30350	0.02	0.00	4.55
…				
70	32330	0.00	0.00	0
sum		(85.7%)	(86.0%)	(77.7%)

5.2 Random vibration Analysis

As mentioned above, the random acceleration load in x-, y-, z-direction on the filter assembly component is defined by a power spectrum density (PSD) diagram which is depicted in Figure 9. These random loads represent one of the load steps which yield relatively high stresses in some parts of the filter assembly, e.g., in x-direction in the spacers. However, no critical stresses have been reported for these load cases. The random vibration analysis was performed with 1% damping ratio (Q=50). One well-known main issue in all linear analyses are edge singularities which occur in nearly 90° concave edges (Figure 10). This numerical singularity cannot be solved by a finer spatial discretization. In a finer discretization the gradients of field variables which are based on a derivation of displacement solution results, would even be higher. One way to handle the problem is the approach to neglect stresses in the direct vicinity of such edges and evaluate solely stresses in a certain distance to the edge (not in the same element). The drawback is, that the real stress peaks at these edges stay unknown. However, a detailed modelling of existing radii between adhesive and housing or spacer cannot be implemented, nor can the physically existing nonlinearity of the adhesive be included due to lack of material data. Due to the large uncertainties regarding the material behavior of the adhesive and other parts, the filter assembly is additionally qualified in experimental environmental tests (Random, Shock and Thermal loads).

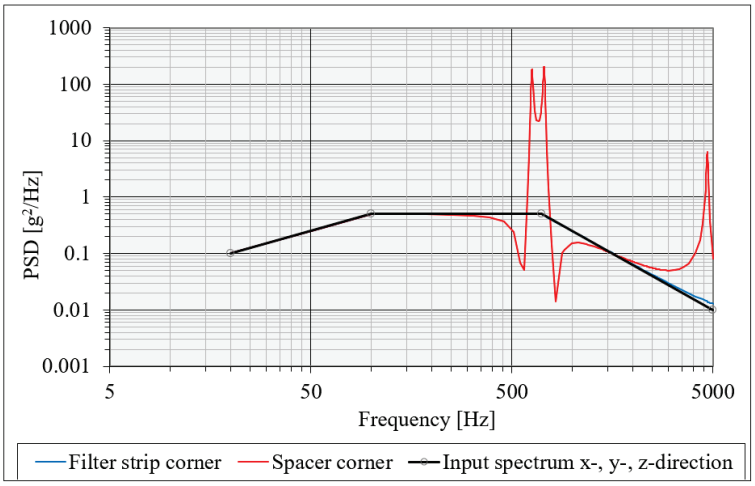

Input spectrum x-, y-, z-directi	
Hz	g^2/Hz
20	1.01E-01
100	0.5
700	0.5
5000	9.93E-03

Figure 9: Input PSD spectrum which was used for the random analyses and the acceleration response PSD spectrum of a corner point (located at a middle filter strip) and a corner point of a spacer (on the middle spacer). For the spacer point, significant acceleration excitations are visible (relevant spacer eigenmodes 625-730Hz) which are a result of the soft fixation by the adhesive.

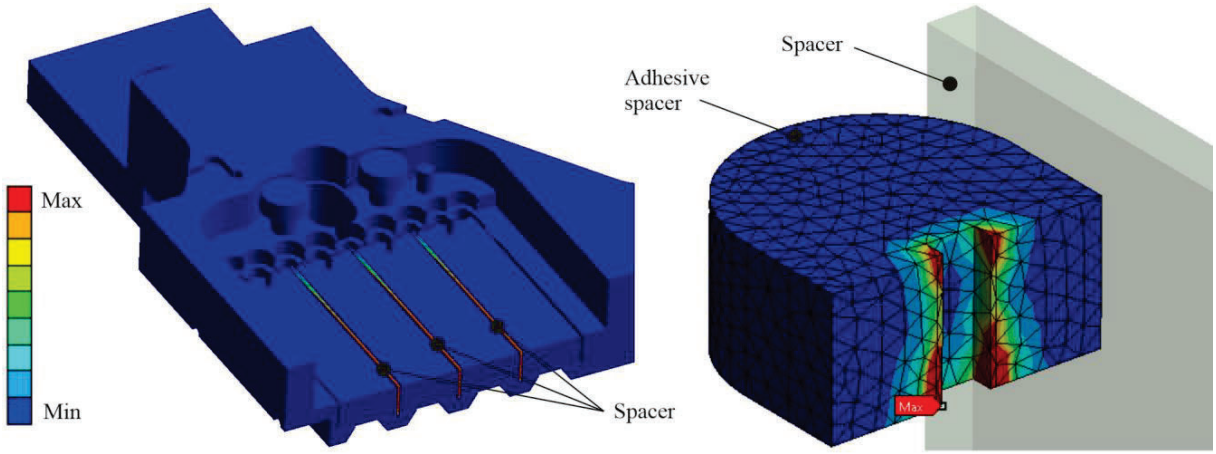

Figure 10: 3-sigma (99.73%) equivalent stresses (Segalman approach) of the random vibration analysis in x-direction. Left: High, but admissible stresses occur in x-direction in the softly suspended spacers (fixed solely by the adhesive). In reality, the spacers will contact the side of the filter stripes which would restrict the maximum deformation and thus the maximum stresses. However, this effect cannot be considered in a linear analysis. Right: Stresses mapping in the adhesive. The stress is heavily influenced by edge singularities. Visibility of some parts is suppressed in both figures.

5.3 Shock Analysis

Similar to the Random vibration analysis, the Shock load analysis – which is performed as a response spectrum analysis – based on a modal analysis of the assembly, too. Modes are excited by the input response spectrum according to their frequencies and participation factors and the modal results are combined using the mode combination method. The Complete Quadratic Combination (CQC) method is an improvement of the square root of Summation of Squares (SRSS) method for the case of closely spaced modes as present in the model (see Table 4). The SRSS method is usually an approach which is too conservative and overestimates the results in models featuring closely spaced modes. As for the

Random analysis, a damping of Q=50 (1%) is used for the Shock analysis which is necessary for the CQC mode combination method. The given input shock response spectrum (SRS) is shown in Figure 11.

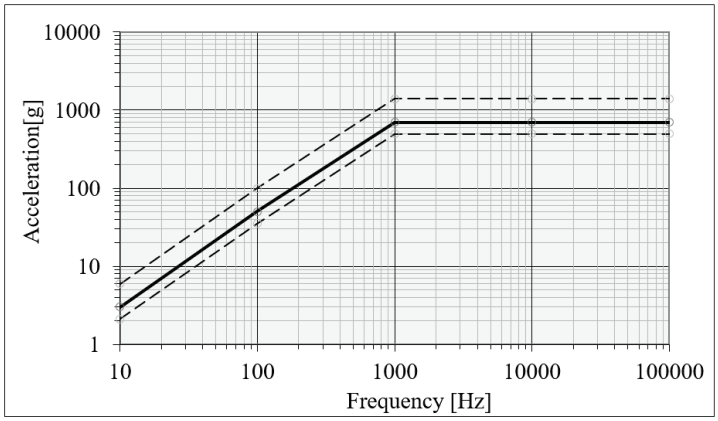

Response spectrum	
Hz	g
10	3
100	50
1000	700
10000	700
100000	700

Figure 11: Used input response spectrum with +6dB and -3dB testing limits (dashed curves).

As a result, a mapping of maximum occurring stresses in the component can be plotted, which is exemplarily shown for z-direction shock loading in Figure 12. Similar to random vibration, an SRS analysis does not provide information about when these maximum stresses occur, because the phase information of the superimposed modes is lost.

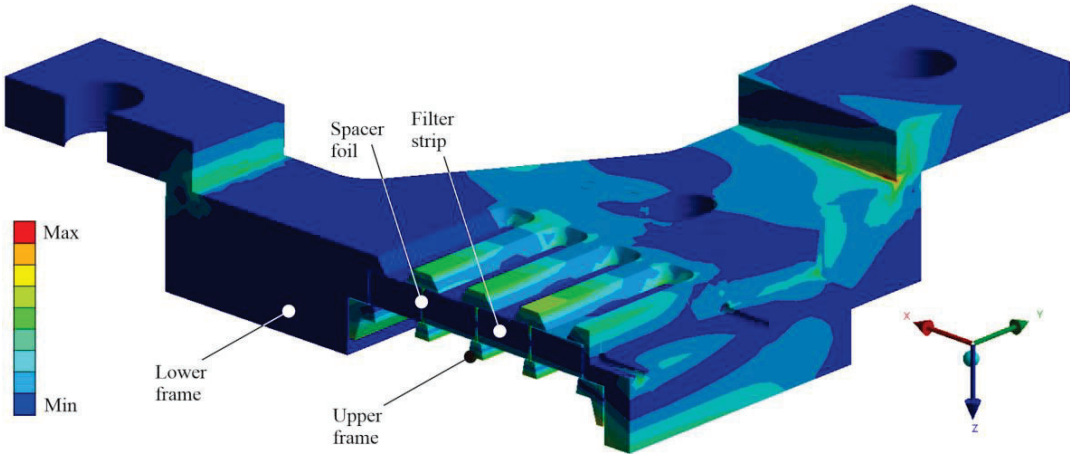

Figure 12: Maximum occurring stress in the SRS analysis from shock loading in z-direction (cross section of filter assembly). Critical points are bending stresses located in an edge to the interfaces (influenced by edge singularities).

However, it should be mentioned that results of response spectrum analyses should generally be regarded with caution as this kind of analysis solely provides an estimation of maximal occurring quantities. To verify the response spectrum analysis of this model, a transient analysis which is based on modal superposition with a synthetically derived transient half sine pulse [4] from the input response spectrum was used. Table 5 gives a comparison of maximum stress results between the random vibration and transient analysis. The deviation between the values is a result of the inadequate approximation of the original SRS by the half sine SRS (Figure 13) and a result of the mode combination method in the response spectrum method. However, despite these deviations it can be stated that the SRS approximation is within an acceptable limit and can be used for a conservative estimation of maximum stresses.

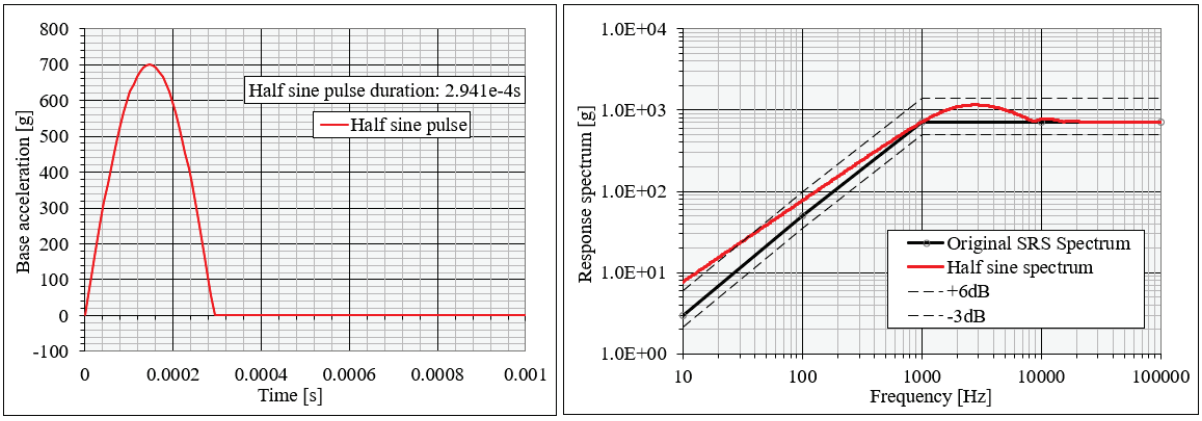

Figure 13: Left: Synthetic transient half sine pulse from the given SRS (black curve in right diagram). Right: Comparison of the SRS between the half sine pulse and the original one.

Table 5: Deviation of maximum stress values from random vibration and transient analysis.

	Filter	Frame	Spacer	Adhesive
Deviation of random vibration analysis to transient analysis	46%	19%	24%	14%

5.4 Thermal analysis

The minimum non-operational temperature, 190K, was also analyzed in a load step. As mentioned above, the thermal model considers geometrical nonlinearity because of the contact of filter stripes and spacer parts to the housing (upper and lower frames) of the assembly. Furthermore, a molybdenum alloy base plate (CTE = 4.77 µm/m/K) was considered for this analysis and the fixation/origin is set symmetric to the fixation of the assembly as visible in Figure 8 right.

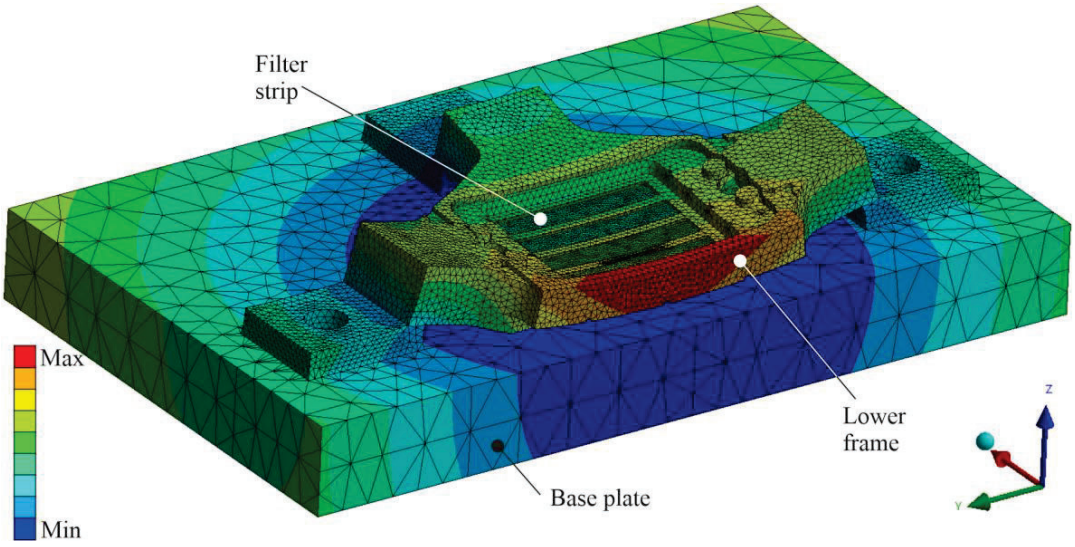

Figure 14: Deformation (scale factor: 150) in the 190K load step. The displacement of the base plate is fixed in three planes which are located as described in Figure 8 right.

As a result from the thermal analyses, the RMS and peak-to-valley deformations of the optical clear apertures of filter stripes have been evaluated for the operational temperature and the maximum occurring forces and moments at the

interfaces. There occur significant shear forces and in-plane moments due to the shrinkage of the titanium frames and the CTE mismatch to the base plate. This shrinkage is also visible in the deformation shape in Figure 14.

5.5 Interface imperfections

To analyze the impact of interface (IF) imperfections on the maximum stress values and interface forces, possible deflections on all interfaces have been investigated. As the model is symmetric to the xz-plane (middle plane between interface #1 and #3), interface deformations must only be applied to one of these interfaces and considered twice in the RMS sum of the interface deformations. Hence, 6 load cases are to be considered: 4 rotations (R_x, R_y at IF #1 and IF#2) and 2 displacements (U_z at IF #1 and IF#2). Figure 15 depicts exemplarily the deformation field and shape for a rotation imperfection at interface #2. All imperfection contributions have been totalized by the square root sum of squares (SRSS) and added to the maximum stresses or forces from the dynamic or thermal load steps.

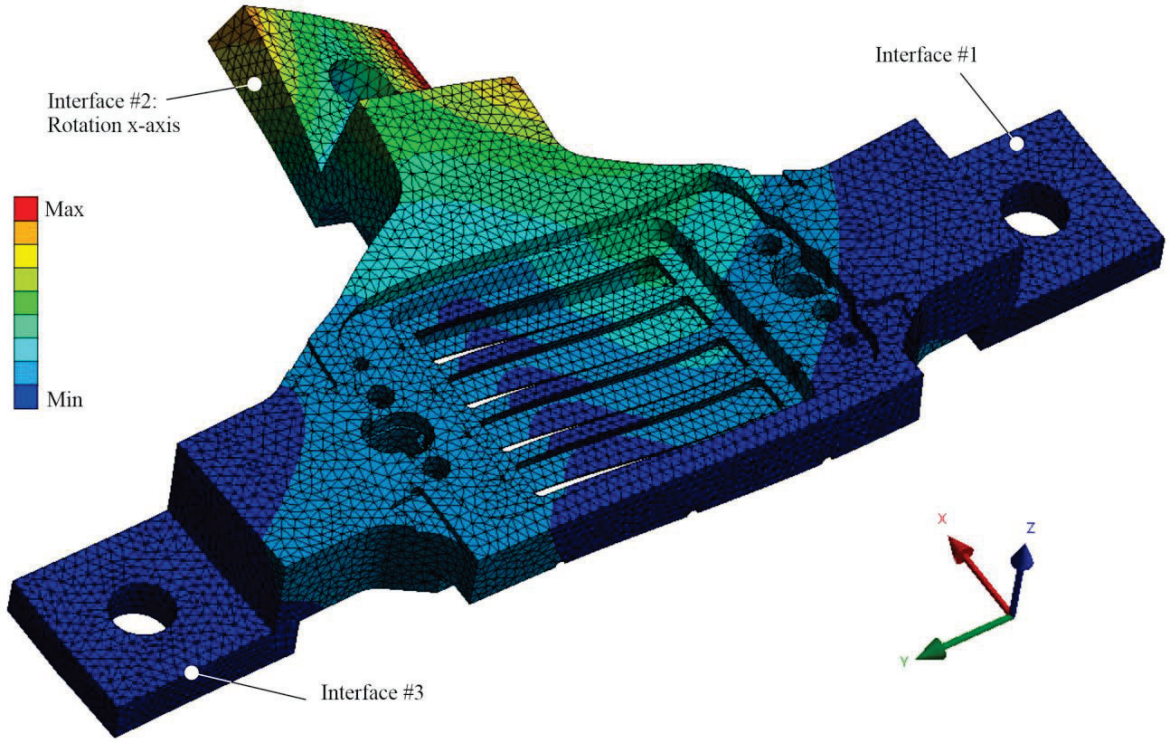

Figure 15: Deformation (scale factor: 1000) due to a rotation of 0.84mrad around x-axis at interface #2.

6. CONCLUSION

Based on the Sentinel S2 SWIR filter assemblies experiences and flight heritage the mechanical design of LSTM DPF-SWIR filter assemblies was developed. The design was adapted to the LSTM mechanical, thermal and optical requirements by changing the filter stripe material and the size and geometry of filter substrates. The mounting of filter substrates into the lower frame of DPF-SWIR filter assemblies is realized by using mechanical stops. All gaps in between the filter stripes and the upper and lower frame mounting structures will be filled by an elastic adhesive for mechanical fixation.

The design was analyzed by thermal and structural FE analysis. 21 load cases of sine and random vibration, shock, thermal environmental loads, interface deformations, and the combination of load cases were analyzed. The results of thermal and structural analysis show the meet of the requirements of the defined environmental loads.

The outcome of thermal and structural analysis will be verified on DPF-SWIR mechanical model in an early stage of the project to meet TRL6.

The working activities of manufacturing and integration of DPF-SWIR mechanical models are in progress and will be finished in quarter III/2022.

7. ACKNOWLEDGEMENTS

The LSTM Filter Assemblies are funded by the European Union and were developed with financial and technical support from and the European Space Agency (ESA) in the frame of the Copernicus Land Surface Temperature Monitoring (LSTM) mission.

REFERENCES

[1] Aibus DS-Toulouse, "Requirement specification LSTM Filter Assemblies (LST-SP-ADST-1000592435_VNIR_SWIR_filters_issue3)
[2] ESA, “Copernicus Sentinel Expansion Mission” (9 August 2022). https://www.esa.int/Applications/Observing_the_Earth/Copernicus/Copernicus_Sentinel_Expansion_missions
[3] Kunz, J., Studer, M., „Druck-Elastizitätsmodul von Elastomeren über Shore-A-Härte ermitteln“, Fachzeitschrift Kunststoffe, 92-94 (6/2006), www.kunststoffe-international.com, Document number PE103590
[4] Irvine, T., „Response of a single-degree-of-freedom system subjected to a classical pulse base excitation“, Revision A, www.vibrationdata.com, 18 Aug. 1999
[5] Schröter, K., Schallenberg, U., Mohaupt, M. „Technological Development of spectral Filters for Sentinel-2.“, International Conference on Space Optics - ICSO 2008, 14-17 October 2008, Proc. Of SPIE Vol. 10566 105662M-1
[6] Chorvalli, V., Espuche, St., Delbru, F., Martimort, P., „The multispectral instrument of the Sentinel2 EM program results“, International Conference on Space Optics - ICSO 2012, 9-12 October 2012, Proc. Of SPIE Vol. 10564 1056408-1
[7] Mohaupt, M., „Manufacturing of high precision Filter Arrays for the Sentinel 2 Satellite“, Euspen 16th international conference and exhibition 2016, https://www.euspen.eu/resource/manufacturing-of-high-precision-filter-arrays-for-the-sentinel-2-satellite/